**Northey T, Penfold T.**

**The intersystem crossing mechanism of an ultrapure blue organoboron emitter.**

***Organic Electronics* 2018, 59, 45-48.**

Organic Electronics 59 (2018) 45–48

Contents lists available at ScienceDirect

Organic Electronics

journal homepage: www.elsevier.com/locate/orgel

# The intersystem crossing mechanism of an ultrapure blue organoboron emitter

T. Northey, T.J. Penfold*

*Chemistry- School of Natural and Environmental Sciences, Newcastle University, Newcastle Upon Tyne, NE1 7RU, United Kingdom*

ARTICLE INFO

*Keywords:*
Thermally activated delayed fluorescence
Quantum dynamics
Organoboron emitter
Intersystem crossing
Spin-vibronic mechanism

ABSTRACT

Quantum dynamics and a spin-vibronic Hamiltonian are used to investigate the intersystem crossing (ISC) mechanism of a narrow organoboron molecular emitter, 5,9-diphenyl-5,9-diaza-13 b-boranaphtho [3,2,1-de] anthracene (**DABNA-1**). We find a rate of ISC ($k_{ISC}$) in good agreement with experiment and which operates via a second-order spin-vibronic coupling mechanism. The nonadiabatic coupling activating this mechanism occurs between the lowest singlet ($S_1$) state and higher lying singlet states promoting ISC into the $T_2$ state. The large $S_1$-$T_1$ energy gap, combined with the slow ISC arising from small spin-orbit coupling and the rigidity of the molecule is the reason for the slow rISC observed experimentally. The importance of the spin-vibronic mechanism, even for narrow Thermally Activated Delayed Fluorescence (TADF) emitters illustrates the importance of identifying the effect of key vibrational modes and their action, when attempting to design molecular emitters combining narrow TADF with efficient rISC.

## 1. Introduction

Organic Light Emitting Diodes (OLEDs) have emerged as an attractive approach for fabricating thinner and more efficient flat panel displays. However, one of the key issues holding OLEDs back is the lack of efficient blue emitters exhibiting working lifetimes of >10,000 h s [1]. This is because the excited states of deep-blue emitters possess very high energy levels, increasing their susceptibility to degradation upon excitation. Consequently, present commercial OLED displays exploit blue emitters with efficiency enhanced by triplet-triplet annihilation, leading to a maximum internal quantum efficiency (IQE) of 62.5% [2].

Thermally Activated Delayed Fluorescence (TADF) offers an alternative approach capable of achieving 100% IQE. By designing an emitter exhibiting a small (≤0.2 eV) energy gap between the low lying singlet and triplets states, it becomes possible to harvest the 75% of the triplet states generated by electrical excitation via delayed fluorescence increasing the efficiency of these devices [3–6]. The most common approach for activating TADF is by exploiting charge transfer (CT) states achieved with donor-acceptor molecules exhibiting a relative orientation near orthogonality. This minimises the electron exchange energy responsible for splitting singlet and triplet states of the same character. However, CT states exhibit an inherently broad and featureless emission. Indeed, the typical full-width at half-maximum (FWHM) of the emission spectrum of a TADF molecule is between 70 and 120 nm. This width reduces the colour purity of the light emitted, undesirable for commercial applications as displays, which require a FWHM <50 nm.

To combat this, Hatakeyama et al. [7] recently proposed a new approach using the resonance effect. By incorporating nitrogen atoms substituted in the para-position relative to a central boron atom, they were able to exploit the opposite resonance effect of the two atoms. The authors demonstrated that using this approach it was possible to reduce the overlap of the highest occupied molecular orbital (HOMO) and lowest unoccupied molecular orbital (LUMO) and therefore the energy gap between the $S_1$ and $T_1$ states to ~0.2 eV, making triplet harvesting via delayed fluorescence feasible. Importantly, this could be achieved without the need of introducing donor and acceptor groups, and two ultrapure blue emitters, 5,9-diphenyl-5,9-diaza-13 b-boranaphtho [3,2,1-de]anthracene (**DABNA-1**, Figure 1) and 9-([1,1′-biphenyl]-3-yl)-N,N,5,11-tetraphenyl-5,9-dihydro-5,9-diaza-13 b-boranaphtho [3,2,1-de]anthracen-3-amine (**DABNA-2**), were reported, which when incorporated into an OLED exhibited a maximum EQE of 25% and an emission FWHM of only 28 nm.

Interestingly, this achievement of a narrow and therefore rigid TADF emitter would appear somewhat opposed to recent work that has shown efficient reverse intersystem crossing (rISC) in TADF molecules is driven by a spin-vibronic mechanism [8–12]. The requirement for specific molecular vibrations to activate this mechanism and activate rISC is likely to add an inherent width to the emission spectra of efficient TADF emitters. Consequently, understanding the (r)ISC

* Corresponding author.
*E-mail address:* tom.penfold@ncl.ac.uk (T.J. Penfold).

https://doi.org/10.1016/j.orgel.2018.04.038
Received 22 March 2018; Received in revised form 20 April 2018; Accepted 23 April 2018
Available online 26 April 2018

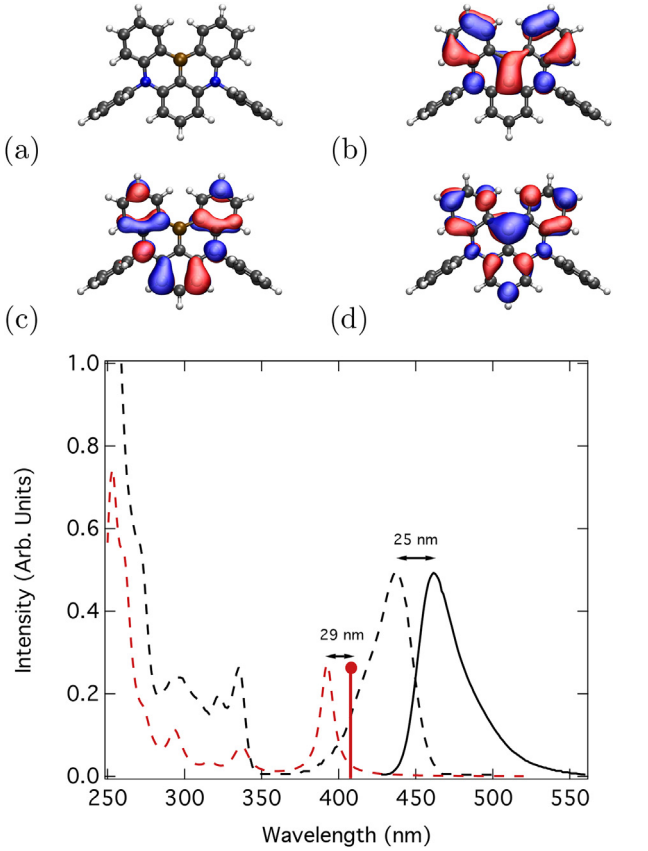


**Fig. 1.** Upper: Molecular structure of **DABNA-1** (a) and the HOMO-1 (b), HOMO (c), and LUMO (d) orbitals. Lower: The calculated (red) and experimental (black) absorption (dashed) and emission (solid) spectra for **DABNA-1**. This spectrum has been generated by broadening each transition with a Lorentzian function with full width half maximum of 5 nm. The experimental spectra have been reproduced from Ref. [7]. (For interpretation of the references to colour in this figure legend, the reader is referred to the Web version of this article.)

mechanism in these narrow boron emitters represents an important step towards achieving rational design of efficient and narrow emitters for OLEDs used in display devices. In this paper we use a model spin-vibronic Hamiltonian and quantum dynamics to study the ISC mechanism of **DABNA-1** (Fig. 1a). All of the computational details can be found in the Supporting information.

## 2. Results

### 2.1. Excited state properties

The geometric and electronic structure of **DABNA-1** has recently been described in Ref. [13] and therefore we only briefly review it here in the interest of clarity and context for the quantum dynamics simulations. Fig. 1 (lower panel) shows the experimental (black dashed) and TDDFT (PBE0) calculated (red dashed) absorption spectrum of **DABNA-1**. The agreement between the two is good, with the exception of the first peak corresponding to the $S_1$ state, for which the calculated value is ~40 nm higher than observed experimentally. This is commonly observed for boron containing molecules [14], and in the context of the present work its effect is to increase the energy gap between the $S_1$ and $S_n$ states. This does not have a significant effect on the dynamics reported below. All transitions visible in the absorption spectrum correspond to $\pi$-$\pi^*$ transitions centred on the boron core of the molecule. The $S_1$ and $T_1$ states are both HOMO→LUMO transitions (Fig. 1). The $T_2$ state is a HOMO-1→LUMO transition and almost degenerate with the $S_1$ at the ground state geometry.

**Table 1**
The magnitude of the spin-orbit coupling matrix elements ($cm^{-1}$) between all relevant states for **DABNA-1** and the thiophene-fused **DABNA** (TF-DABNA) calculated using the one-electron Breit-Pauli Hamiltonian within the framework of TDDFT (PBE0) as implemented within the Q-Chem quantum chemistry package [15].

| States | SOCME ($cm^{-1}$) | |
|---|---|---|
| | **DABNA-1** | **TF-DABNA** |
| $T_1$-$S_0$ | 0.66 | 0.89 |
| $T_1$-$T_2$ | 1.17 | 2.10 |
| $S_1$-$T_1$ | 0.13 | 0.27 |
| $S_1$-$T_2$ | 0.04 | 1.53 |
| $S_2$-$T_1$ | 2.03 | 1.83 |
| $S_2$-$T_2$ | 0.65 | 0.81 |
| $S_3$-$T_1$ | 1.31 | 0.96 |
| $S_3$-$T_2$ | 0.21 | 0.14 |
| $S_4$-$T_1$ | 1.39 | 0.97 |
| $S_4$-$T_2$ | 0.38 | 1.49 |

The emission spectrum, i.e. the energy of the $S_1$ state at its relaxed geometry, is also shown in Fig. 1. The Stokes shift, corresponding to the structural change between the Franck-Condon geometry and the optimised $S_1$ geometry is only 29 nm, in good agreement with the experiment [7]. As observed for the absorption spectrum, the $S_1$ energy relative to the ground state is overestimated by ~ 40 nm. The structural changes associated with this Stokes shift correspond to a slight shortening of the bond lengths around the boron and a flattening of the phenyl rings, as observed in Ref. [13]. As illustrated by the small Stokes shift, these structural changes are very small. The oscillator strength ($f$) of the $S_1$ excited state at the excited state geometry is 0.187, which is significantly larger than TADF molecules based upon CT states [16].

The spin-orbit-coupling matrix elements (SOCME) of **DABNA-1**, calculated at the ground state optimised geometry are shown in Table 1. These are small in all cases, especially for the important $S_1$-$T_2$ states. Due to the rigidity of **DABNA-1**, these coupling elements are only weakly dependent on the excited state structural changes of the molecule. Importantly, because these values are small and need to be improved in order to increase the singlet-triplet coupling in the organoboron emitters. One potential approach is adopting thiophene-fused structure [17] similar to that used recently to develop a heavy-atom-free BODIPY triplet photosensitisers. To assess this, Fig. 2 shows the structure and HOMO and LUMO orbitals of a proposed asymmetric thiophene-fused derivative of DABNA. The SOCME are shown in Table 1 and a notable increase is observed, most pertinently between the $S_1$-$T_2$ states, which is almost two orders of magnitude larger.

### 2.2. Quantum dynamics

These excited state properties are now used to inform the development of a model spin-vibronic Hamiltonian, as described in the Supporting information. This is subsequently used to perform quantum dynamics and reveal the mechanism of ISC in **DABNA-1**. Fig. 3a shows the population kinetics of the triplet states ($T_1 + T_2$) obtained from 100 ps of these quantum dynamics simulations after impulsive excitation into the $S_1$ state from the Franck-Condon geometry in the ground state. The blue dashed line corresponds to a simulation for which only the $S_1$, $T_1$ and $T_2$ states have been included. This shows extremely slow population transfer into the triplet states. Using the gradient of these population kinetics, $k_{ISC}$ is estimated to be ~$10^3$ $s^{-1}$. However, it is emphasised that the timescale of the dynamics is very short compared to this rate. Although this value should only be used as a qualitative estimate, it is in broad agreement with recent calculations of $k_{ISC}$ [13]. Most pertinently, both of these calculated rates are 2–3 orders of magnitude smaller than reported from experiment in Ref. [7], 4.5×$10^6$$s^{-}$

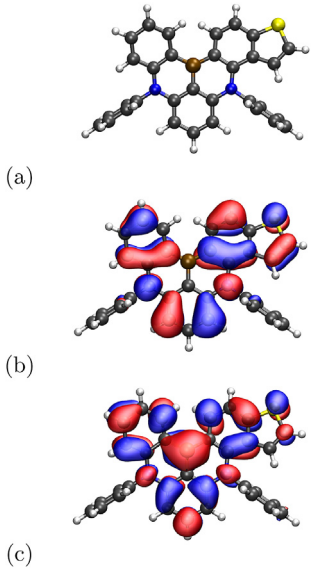


**Fig. 2.** Molecular structure of asymmetric thiophene fused DABNA derivative (a) and the HOMO (b), LUMO (c) orbitals.

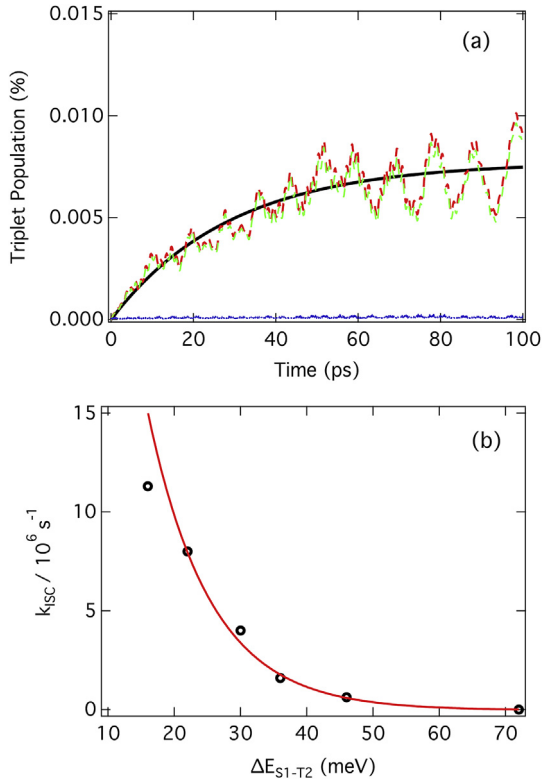


**Fig. 3.** (A) The percentage of the wavepacket populating the triplet states [$T_{1,2}$] of **DABNA-1** with (red) and without (green) the $T_1$ state for 100 ps of excited state dynamics after impulsive excitation into the $S_1$ state. The black line is a fit of the population kinetics yield $k_{ISC} = 8.0\times10^6\,s^{-1}$. The blue line corresponds to a simulation for which only the $S_1$, $T_1$ or $T_2$ states have been included and shows very slow populations kinetics. (b) Calculated $k_{ISC}$ as a function of the $S_1$-$T_2$ energy gap. (For interpretation of the references to colour in this figure legend, the reader is referred to the Web version of this article.)

[1], and therefore something is clearly missing.

The red trace in Fig. 3a shows the population kinetics of the triplet states ($T_1 + T_2$) for the full model Hamiltonian, which includes coupling of the $S_1$ state to the higher lying singlet ($S_{2\text{-}4}$) states. In comparison to the blue trace, a significant enhancement of $k_{ISC}$ is observed. A fit of this population kinetics yields $k_{ISC} = 8.0\times10^6\,s^{-1}$, in excellent agreement with the experimentally determined rate reported in Ref. [7]. The rate enhancement derives from the stronger SOC of the higher lying singlet states with the low lying triplet states compared to the $S_1$ state (Table 1). This, in conjunction with the coupling between the $S_1$ and higher lying singlet states, derived from vibrational modes including torsions of the phenyl rings and antisymmetric stretches of the boron core, increases the mixing between the singlet and triplet manifolds enhancing $k_{ISC}$. These simulations show, in agreement with other recent work [9–11] that ISC operates via a spin-vibronic mechanism. In this case, these higher lying singlet states can be described as virtual intermediate states in the sense that they enhance the population transfer without receiving significant population themselves. This is similar to the superexchange mechanism reported for singlet fission [18].

**DABNA-1** operating via a spin-vibronic mechanism highlights a crucial tension for efficient TADF emitters seeking to achieve narrow FWHM of the emission. The spin-vibronic mechanism is promoted by off-diagonal intra-state coupling terms expressed [8]:

$$W_{ij}^{(1)} = \sum_{\alpha} \left\langle \Phi_i(\mathbf{Q}_0) \left| \frac{\partial \hat{\mathcal{H}}_{el}}{\partial Q_\alpha} \right| \Phi_j(\mathbf{Q}_0) \right\rangle Q_\alpha \tag{1}$$

Therefore it follows that the larger the displacement in $Q$, the larger the effect of coupling is. For typical D-A systems, the conformational freedom provides an efficient route for activating this coupling via conformational flexibility along important nuclear degrees of freedom ($Q$), but these also are directly or indirectly responsible for the inherently broad emission. In contrast, **DABNA-1** exhibits a narrow emission, but because of this rigidity the effectiveness of the spin-vibronic coupling mechanism is reduced. This is a key contributing factor in the slow ISC compared to other all organic systems [19,20].

Important in the context of triplet harvesting via TADF, the green trace shows the same simulation, with the population of the $T_1$ state removed. Therefore, although some phosphorescence from the $T_1$ state is observed at low temperatures in solid matrices, this reveals that coupling to it has little effect on influencing $k_{ISC}$, consistent with the larger energy gap and weak coupling. Fig. 3b shows the $k_{ISC}$ as a function of the $S_1$-$T_2$ energy gap, which as expected from first or second order rate equations, shows exponential dependence [8].

While the $S_1$-$T_2$ energy gap is clearly more important than the position of the $T_1$ state for ISC, this will obviously not be the case during rISC. Using the $\Delta E_{S1\text{-}T1} = 0.15$ eV energy gap for the **DABNA** complexes recently reported in Ref. [21], the $k_{rISC}$ can be determined directly, from both our calculated and the experimental [7] $k_{ISC}$ using a Boltzmann distribution to determine probability of overcoming the large energy barrier. This is indicative of a rISC mechanism controlled from the coupling between the $T_2$ and $S_1$ states, and whose rate is limited by the energy gap to the lower lying $T_1$ state (Fig. 4).

As a final note, while our present simulations are consistent with the rISC reported experimentally, they do not study it directly. In terms of the triplet harvesting mechanism of **DABNA-1**, it is also interesting to note that the $k_{rISC}$ of **DABNA-2** [7,21] appears to be dependent on the concentration of the emitter within the host. Indeed $k_{rISC}$ decreases by almost an order of magnitude for 6% by weight in mCBP compared to 1%. This is suggestive of host involvement in the triplet harvesting mechanism. This could be an implicit effect, changing guest-host interactions, or explicit in the sense that triplet excitons generated on the host could be transferred via a Dexter mechanism into the $T_2$ of the **DABNA-1**. The latter, if controlled, could provide a route of triplet harvesting, which avoids the low lying $T_1$ state. A detailed study of the energy transfer mechanism for guest-host blends would be required to untangle this. In addition, the slow rate of rISC is likely to put it in competition with triplet quenching mechanisms and should be carefully considered when concluding on likely device performance.

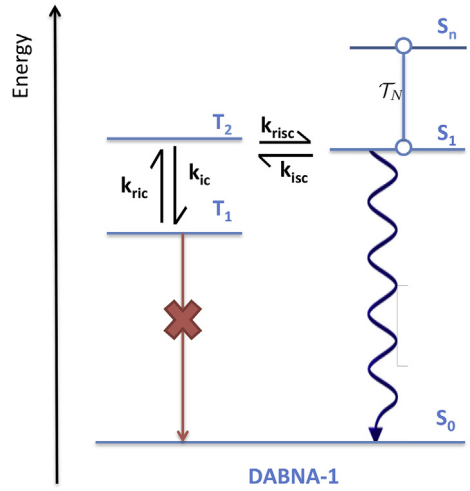


**Fig. 4.** Schematic of the ISC mechanism and triplet harvesting in **DABNA-1**. Singlet-triplet mixing is enhanced by coupling to virtual singlet states. While there are two possible triplet states ($T_1$ and $T_2$), which can be populated, the latter is favoured due to the small energy gap and stronger coupling.

## 3. Conclusions

In summary, we have used quantum dynamics to demonstrate that despite adopting a novel design approach, the (r)ISC mechanism in **DABNA-1** like other organic emitters used for OLEDs, operates via a second-order spin-vibronic coupling mechanism. In this case, it is the nonadiabatic coupling between the $S_1$ and higher lying singlet states which facilitates the spin-state change. These higher-lying singlet states can be described as virtual intermediate states in the sense that they enhance the population transfer without receiving significant population themselves. Importantly, the ISC in **DABNA-1** can be described without including the $T_1$ state. Indeed, it operates mostly via the $T_2$-$S_1$ states, due to the energetic proximity.

Crucially, the application of the **DABNA** derivatives in OLEDs [7] or as TADF laser dyes [21] is currently limited by the rate of triplet harvesting. Therefore acceleration of $k_{rISC}$ is essential. An obvious approach would be to decrease $\Delta E_{S1\text{-}T1}$, although this is likely to be challenging, especially if one wishes to avoid introducing CT character and avoid reducing the radiative rate. The SOCMEs in the **DABNA** derivatives are small and could perhaps, as shown, be enhanced by adopting the thiophene-fused approach [17]. Given the spin-vibronic mechanism, potentially the most promising approach for progressing the design of these materials is to increase the emphasis on identifying the vibrational modes responsible for promoting reverse intersystem crossing and broadening the FWHM of the emission. Understanding these key interconnecting factors will make it possible to develop molecular design which includes vibrational modes, enhancing the former without contributing to the latter.

## Conflicts of interest

The authors declare no competing financial interests.

## Data availability

Data supporting this publication is openly available under an "Open Data Commons Open Database License". Additional metadata are available at: 10.17634/153015-5. Please contact Newcastle Research Data Service at rdm@ncl.ac.uk for access instructions.

## Acknowledgements

The EPSRC are acknowledged for funding through Project EP/N028511/1.

## Appendix A. Supplementary data

Supplementary data related to this article can be found at http://dx.doi.org/10.1016/j.orgel.2018.04.038.

## References

[1] H. Nakanotani, T. Higuchi, T. Furukawa, K. Masui, K. Morimoto, M. Numata, H. Tanaka, Y. Sagara, T. Yasuda, C. Adachi, Nat. Commun. 5 (2014) 4016.
[2] C.-J. Chiang, A. Kimyonok, M.K. Etherington, G.C. Griffiths, V. Jankus, F. Turksoy, A.P. Monkman, Adv. Funct. Mater. 23 (2013) 739–746.
[3] M.Y. Wong, E. Zysman-Colman, Adv. Mater. 29 (2017) 1605444.
[4] Z. Yang, Z. Mao, Z. Xie, Y. Zhang, S. Liu, J. Zhao, J. Xu, Z. Chi, M.P. Aldred, Chem. Soc. Rev. 46 (2017) 915–1016.
[5] F.B. Dias, T.J. Penfold, A.P. Monkman, Methods Appl. Fluoresc. 5 (2017) 012001.
[6] T.J. Penfold, F. Dias, A.P. Monkman, Chem. Commun. 54 (2018) 3926–3935.
[7] T. Hatakeyama, K. Shiren, K. Nakajima, S. Nomura, S. Nakatsuka, K. Kinoshita, J. Ni, Y. Ono, T. Ikuta, Adv. Mater. 28 (2016) 2777–2781.
[8] T. Penfold, E. Gindensperger, C. Daniel, C. Marian, Chem. Rev. (2018), http://dx.doi.org/10.1021/acs.chemrev.7b00617.
[9] J. Gibson, A. Monkman, T. Penfold, ChemPhysChem 17 (2016) 2956–2961.
[10] J. Gibson, T. Penfold, Phys. Chem. Chem. Phys. 19 (2017) 8428–8434.
[11] M.K. Etherington, J. Gibson, H.F. Higginbotham, T.J. Penfold, A.P. Monkman, Nat. Commun. 7 (2016) 13680.
[12] C.M. Marian, J. Phys. Chem. C 120 (2016) 3715–3721.
[13] L. Lin, J. Fan, L. Cai, C.-K. Wang, Mol. Phys. (2017) 11919–11928.
[14] M.R. Momeni, A. Brown, J. Chem. Theor. Comput. 11 (2015) 2619–2632.
[15] Y. Shao, L.F. Molnar, Y. Jung, J. r. Kussmann, C. Ochsenfeld, S.T. Brown, A.T.B. Gilbert, L.V. Slipchenko, S.V. Levchenko, D.P.O. Neill, R.A. DiStasio Jr., R.C. Lochan, T. Wang, G.J.O. Beran, N.A. Besley, J.M. Herbert, C. Yeh Lin, T. Van Voorhis, S. Hung Chien, A. Sodt, R.P. Steele, V.A. Rassolov, P.E. Maslen, P.P. Korambath, R.D. Adamson, B. Austin, J. Baker, E.F.C. Byrd, H. Dachsel, R.J. Doerksen, A. Dreuw, B.D. Dunietz, A.D. Dutoi, T.R. Furlani, S.R. Gwaltney, A. Heyden, S. Hirata, C.-P. Hsu, G. Kedziora, R.Z. Khalliulin, P. Klunzinger, A.M. Lee, M.S. Lee, W. Liang, I. Lotan, N. Nair, B. Peters, E.I. Proynov, P.A. Pieniazek, Y. Min Rhee, J. Ritchie, E. Rosta, C. David Sherrill, A.C. Simmonett, J.E. Subotnik, H. Lee Woodcock III, W. Zhang, A.T. Bell, A.K. Chakraborty, D.M. Chipman, F.J. Keil, A. Warshel, W.J. Hehre, H.F. Schaefer III, J. Kong, A.I. Krylov, P.M.W. Gill, M. Head-Gordon, Phys. Chem. Chem. Phys. 8 (2006) 3172.
[16] T. Northey, J. Stacey, T. Penfold, J. Mater. Chem. C 5 (2017) 11001–11009.
[17] S. Ji, J. Ge, D. Escudero, Z. Wang, J. Zhao, D. Jacquemin, J. Org. Chem. 80 (2015) 5958–5963.
[18] S.R. Yost, J. Lee, M.W. Wilson, T. Wu, D.P. McMahon, R.R. Parkhurst, N.J. Thompson, D.N. Congreve, A. Rao, K. Johnson, et al., Nat. Chem. 6 (2014) 492–497.
[19] I. Lyskov, C.M. Marian, J. Phys. Chem. C 121 (2017) 21145–21153.
[20] V. Rai-Constapel, T. Villnow, G. Ryseck, P. Gilch, C.M. Marian, J. Phys. Chem. 118 (2014) 11708–11717.
[21] H. Nakanotani, T. Furukawa, T. Hosokai, T. Hatakeyama, C. Adachi, Adv. Opt. Mater. 5 (2017) 1700051.